



Versatile 126–182 GHz UWB D-Band FMCW Radar for Industrial and Scientific Applications

Simon Kueppers¹, Timo Jaeschke¹, Nils Pohl^{2,*} , and Jan Barowski^{3,*} 

¹2π LABS GmbH, Bochum, Germany

²Institute of Integrated Systems, Ruhr University Bochum, 44801 Bochum, Germany

³Institute of Microwave Systems, Ruhr University Bochum, 44801 Bochum, Germany

*Senior Member, IEEE

Manuscript received November 7, 2021; accepted November 19, 2021. Date of publication November 25, 2021; date of current version December 22, 2021.

Abstract—In this letter, a D-band frequency-modulated continuous wave (FMCW) radar for industrial and scientific applications is presented. It covers an ultrawide 56 GHz sweep bandwidth (126–182 GHz, 36.4%) and is based on a custom 1 TRX + 2 RX SiGe transceiver millimeter-wave (mmW) integrated circuit manufactured in Infineon's B11HFC 130 nm BiCMOS process with an f_T of 250 GHz and f_{max} of 370 GHz. An innovative versatile multichannel edge-launch waveguide frontend-module architecture allows covering applications requiring dual polarization sensing or azimuth and elevation angle-of-arrival estimation based on the same mmW circuit board. The FMCW sweeper is based on measurement equipment grade commercial fractional-N PLL synthesizers in an offset dual-loop configuration for highly linear wideband FMCW sweep generation with a phase noise of better than -80 dBc/Hz ($f_{off} > 10$ kHz) and superior performance even for ultrafast ramp slopes of more than 56 GHz/1 ms. Intermediate frequency signals of a single target measurement are presented to demonstrate the dynamic range capabilities of the FMCW radar. An SNR of 81 dB is achieved using a metal plate reflector target in free space. Due to the ultrawide bandwidth and the resulting calibrated range resolution of 2.7 mm (-3 dB width, Tukey window), target separation is even possible in dense multitarget environments. Additionally, synthetic aperture radar images are presented as an example application utilizing the high-range resolution capabilities.

Index Terms—Microwave/millimeter wave sensors, BiCMOS, D-band, millimeter-wave (mmW) radar, radar imaging, ultrawideband radar.

I. INTRODUCTION

In comparison to expensive and bulky lab instrumentation devices, such as vector network analyzers (VNAs), frequency-modulated continuous wave (FMCW) sensors allow for a higher degree of flexibility and improved robustness, due to the high level of integration. Therefore, they offer advantages in harsh industrial environments [1] or when a mobile or scanning operation is required [2]. Furthermore, the FMCW principle allows for faster sweep times, making measurements in dynamic environments feasible [3]. Of course, this comes at the cost of a reduced dynamic range, when compared to high-end VNA instrumentation, which is still more than sufficient for most industrial sensing tasks [4]. Latest developments in radio frequency regulatory bodies, such as FCC (USA), Ofcom (U.K.), and CEPT/ETSI (EU), show the rising interest in making spectrum available in the frequency range above 116 GHz to allow new and innovative industrial sensing applications. Recently, FCC opened 21.2 GHz of total bandwidth in the frequency bands 116–123 GHz, 174.8–182 GHz, 185–190 GHz, and 244–246 GHz for unlicensed use. In CEPT, a similar work is ongoing, with the prospect of even wider frequency bands allowed to be used in the European Union, soon. Especially the radio determination industrial in shielded environments (RDI-S) device class in CEPT work item WI71 (ECC Report 334) is supposed to allow covering more than 56 GHz of contiguous bandwidth in the frequency range from 126 to 182 GHz with industrial radar devices for the first time. This enables future radar devices to perform ultrawideband frequency



Fig. 1. Photographs of the FMCW radar sensor with dielectric lens antenna (left) and WM-1651 (WR6) waveguide flange (right).

response measurements for a large variety of applications [5]–[9], such as classical VNAs.

Fig. 1 shows a photograph of the here presented sensor with a dielectric lens antenna (left) mounted on a WM-1651 (WR6) waveguide flange. The backend is realized using integrated switched dual-port GbE interfaces, and power is supplied by a 24–48 V (typ.) input or Power-over-Ethernet. The following sections focus on the transceiver millimeter-wave integrated circuit (MMIC), frontend module, and millimeter-wave (mmW) radar system details, and present measurements to highlight the performance of the sensor system. The main contribution of this letter is to highlight the achieved record bandwidth of 56 GHz in a combination with a fast chirp rate of 1 ms and the high signal-to-noise ratio and frequency/phase stability. Additionally, we present an innovative configurable edge-launch mm-W sensor design that can support dual polarization reception or multiple separate RX channels to highlight the potential of such sensor systems for

Corresponding author: Jan Barowski (email: jan.barowski@rub.de).

Associate Editor: Jesus M. Corres.

Digital Object Identifier 10.1109/LENS.2021.3130709

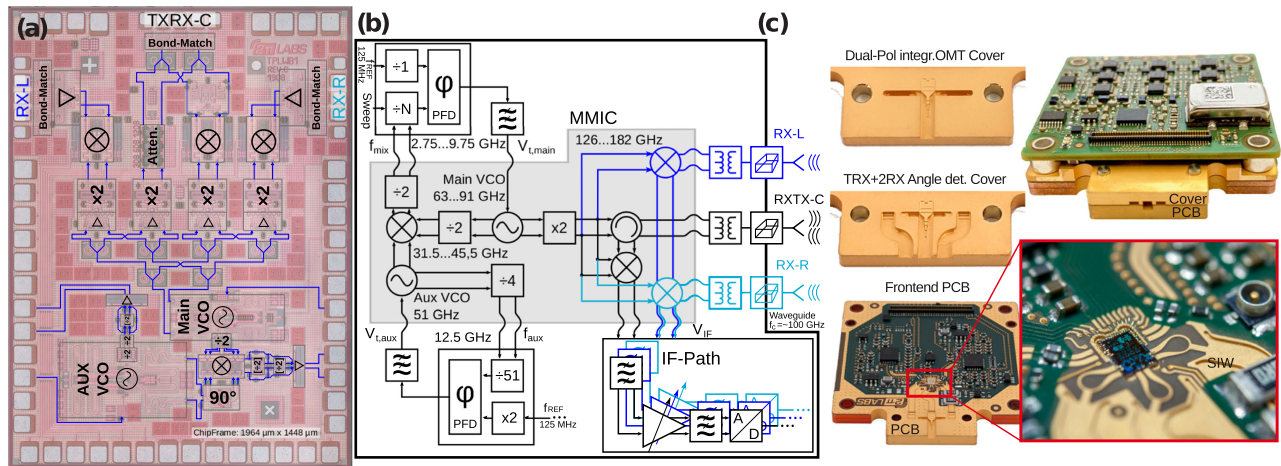


Fig. 2. (a) SiGe MMIC with auxiliary voltage-controlled oscillator (VCO), fundamental 63–91 GHz sweep VCO, Gilbert frequency doublers to 126–182 GHz, single transceiver (TXRX-Center), and dual receiver (RX-Left/RX-Right) channels. (b) Dual-loop offset PLL configuration system block diagram. (c) Edge-launch waveguide mmW frontend module with different function-covers for (i) dual-polarization measurement with embedded OMT and (ii) with centered TXRX-channel and two additional RX channels. Differential signals are converted to single ended using baluns, then fed into SIW structures and finally into PCB-embedded air-filled waveguides.

demanding applications, such as precision ranging, material characterization, or radar imaging.

II. SYSTEM DETAILS

In this section, further details on the MMIC and system concept and the mmW frontend module are presented.

A. D-Band Transceiver MMIC and System Concept

The core component of the sensor platform is a custom transceiver SiGe MMIC with two additional RX channels, manufactured in Infineon's B11HFBC BiCMOS technology [10]. Fig. 2(a) shows a chip micrograph with detailed component and signal path annotation. An offset-phase-locked loop (PLL) concept is utilized for stabilizing and sweeping the ultrawideband 63 to 91 GHz fundamental VCO, similar to [11]. The generated signal is divided by 2 and then single-sideband mixed in reverse position with a second PLL-stabilized static auxiliary VCO at 51 GHz. This arrangement allows for stable and excellent phase noise performance over the entire sweep bandwidth, because the PLL's fractional ratio can be chosen smaller (see [12]). The radar output signal is then generated by doubling the frequency of the generated fundamental VCO signal using bootstrapped Gilbert cell frequency doublers [13].

The covered bandwidth Δf of the MMIC from 126 to 182 GHz in a combination with highly linear PLL stabilized frequency sweeps results in a calibrated range resolution of

$$\delta_{\text{range, -3dB, Tukey}} = \frac{c_0}{2 \cdot \Delta f} \cdot c_w = 2.7 \text{ mm} \quad (1)$$

with c_0 being the speed of light, and a factor $c_w = 1.01$ to compensate for the influence of the here used Tukey windowing function.

An output power of ≈ 3 dBm is achieved at the chip. The chip components have been optimized for minimum intermediate frequency (IF) signal variation over the entire sweep bandwidth taking into account all system-level components. A total occupied chip area of 2.84 mm was achieved through a high level of integration and maximum chip area utilization. Sufficient isolation between adjacent

channels is maintained by placing the RX channels at 90° angle from the TXRX channel.

A high RX and TX signal separation better than 15 dB of the transceiver channel is achieved using lumped element Wilkinson splitters. Especially, the lumped element resistor has been specifically optimized in size and low parasitic impedance to achieve good isolation performance between the isolated ports. The separated receive signal is then fed into Gilbert cell downconversion mixers.

All three channels use compensation networks to reduce the impact of the pad capacitance and differential bond wires, which has proven to be sufficiently reproducible for commercial applications with standard manufacturing techniques and over the entire bandwidth. The power consumption of the MMIC with all channels enabled is 1 W from a single 3.3 V supply.

Fig. 2(b) shows the high-frequency block diagram. External commercially available high-end PLL synthesizer chips [14] are used to lock the VCOs on the MMIC to a high-quality 125 MHz reference clock resulting in good phase noise performance and long-term signal stability in all frequency regions.

B. Frontend Technology and Concept

A crucial core component of the D-band FMCW radar is the mmW frontend comprising all high-frequency components in a robust module. In Fig. 2(c), a photograph of the module with an edge-launch waveguide is shown. All high-frequency components, such as the SiGe transceiver MMIC, differential microstrip to substrate-integrated waveguide (SIW) transitions, and SIW to air-filled waveguide transitions, are located on a 127- μm -thick Rogers RT5880 laminate. The laminate includes an additional thick bottom copper cladding for mechanical stability and excellent thermal performance. Additionally, one-half of the RF waveguide structure is embedded in the PCB production process into the thick bottom copper layer. The second-half of the waveguide structure is milled into the top cover, which also serves as an enclosure to protect parts of the module, such as the MMIC and bond wires. The TXRX and RX channels are arranged to allow flexible configuration of the frontend by simply changing the cover to realize different functionalities. One cover variant [see Fig. 2(c) top left] provides reception in both polarizations using an embedded

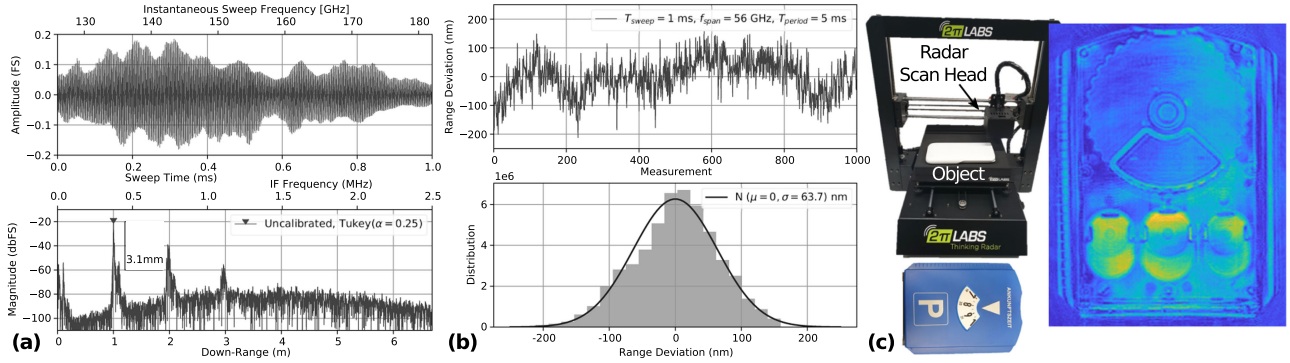


Fig. 3. (a) Measured IF signal of a metal plate target in 1 m distance with a 1 ms FMCW sweep from 126 GHz to 182 GHz and the corresponding range profile with a dynamic range of 81 dB. (b) Target phase jitter of 1000 consecutive measurements. (c) SAR-image obtained from a X/Y gantry stage. The image shows a parking disc as an example for a thin layered object.

TABLE I. Comparison of the State-of-the-Art Wideband Radar Systems in the D-Band

Ref.	Year / Name	TRX/TX/RX # / # / #	Frequency (GHz)	Bandw. (GHz)	P_{TX} (dBm)	Phase Noise (dBc/Hz)	Chip area (mm^2)	Notes (Type/Antenna)
[15]	2021 Hansen et al.	1/0/0	122 - 175	53	-10 (WG)	-70 (in-loop)	—	Bond \rightarrow SIW \rightarrow WG
[16]	2021 Ahmad et al.	0/1/1	154 - 162	8	13 (on-chip)	—	5.43	Cascadable chip
[17]	2021 Visweswaran et al.	0/2/1	138 - 151	13	8.5 (EIRP)	-86.9 (1 MHz)	7.1	On chip antenna
[18]	2020 Küppers et al.	0/N/N	119 - 124	5	4 (on-chip)	-94 (1 MHz)	9	MIMO ICs TX+RX
[19]	2020 Kucharski et al.	1/0/0 & 0/1/1	158 - 178	20	8-18 (EIRP)	-96 (in-loop)	5.4	Mono/Bi ICs, on chip ant.
[20]	2019 Issakov et al.	0/1/3	117 - 126	9	8 (EIRP)	-93.6 (1 MHz)	9.6	
[21]	2017 Hitzler et al.	0/1/1	148 - 162	16	11 (EIRP)	-89 (1 MHz)	2	On chip antenna (DRA)
[22]	2017 Furqan et al.	0/1/1	116 - 146	30	11 (on-chip)	—	3.85	
[23]	2016 Frischen et al.	1/0/0	122 - 123	1	—	-83 (10 kHz)	2.7	Antenna-In-Package
[24]	2014 Jaeschke et al.	1/0/0	122 - 170	48	-1 (on-chip)	-80 (in-loop)	3.86	
[25]	2014 Girma et al.	2/0/0	114 - 124	10	—	—	≈ 5	Chip ant. & QFN package
	This Work	1/0/2	126 - 182	56	-8 (WG)	-80 (10 kHz)	2.84	Bond \rightarrow SIW \rightarrow WG

orthomode transducer (OMT) allowing, for e.g., polarimetric SAR, as shown in [26]. Another variant [see Fig. 2(c) center left] allows for the estimation of direction of arrival (azimuth and elevation) or waveguide transmission setup applications with two additional RX waveguide ports at the frontend board edge.

The edge launch frontend module is suited to directly feed dielectric lens antennas [27]. The realized antenna gain can easily be changed by different antenna sizes. Alternatively, a UG-387/U flange adapter allows to access all ports with standard WM-1651 [28] waveguide equipment.

III. APPLICATIONS AND MEASUREMENT EXAMPLES

To validate the performance of the sensor system, range-, jitter-, and a high-resolution SAR measurements are presented.

A. Single-Target IF Data, Range Profile, and Jitter

To evaluate the radar performance and to present the round-trip amplitude shape, an acquired raw IF signal of a flat reflector target in 1 m distance for a full-bandwidth sweep of 56 GHz in 1 ms is shown in Fig. 3(a). The IF envelope variation across the entire bandwidth shows the excellent frequency response matching of all RF components, such as transmitter, antenna gain, and receiver, on the system level and is smaller than a factor of 5. The corresponding range profile, acquired

using a windowed FFT, shows an achieved dynamic range of 81 dB with 1 ms measurement time and an uncalibrated -3 dB peak-width of 3.1 mm. Fig. 3(b) shows the residual random-phase jitter of the single target measurement in 1 m distance over 1000 measurements. The jitter closely follows a normal distribution with a standard deviation of 63.7 nm.

B. Hi-Res SAR Imaging Setup

Fig. 3(c) shows a synthetic aperture radar (SAR) image obtained with the UWB radar sensor and an open waveguide antenna as a scanning head on a X/Y stage. 3-D-SAR applications and especially thin objects-under-test, such as the parking time indicator disc, highly benefit from the high-range resolution. Alongside the high azimuth resolution provided by the wavelength, high-quality images are obtained. Scanning the object from above allows layer-by-layer evaluation of the different plastic components. The GPU back-projection [29] processed SAR image of the acquired nonfocused IF datasets has an image resolution of $\approx 1 \text{ mm} \times 1 \text{ mm} \times 2.7 \text{ mm}$ (X/Y/Z). The in-depth resolution is limited by the system bandwidth, and the XY resolution depends on the open-waveguide aperture size, i.e., the opening angle. The rotatable disc inside the enclosure, the grooves along the circumference, and three spare shopping-cart tokens can clearly be resolved, allowing for nondestructive testing and end-of-line tests. This imaging technique can also be used to extract spatial material parameters, as shown in [30] and [31].

IV. CONCLUSION

A wideband D-band FMCW radar technology platform using a custom-designed SiGe MMIC was presented. The single transceiver and dual receiver SiGe-IC achieves (to the best of our knowledge, cf., Table 1) a best-in-class bandwidth of 56 GHz. Its flexible architecture allows for angle- and polarization-detection applications, whilst maintaining the highest measurement precision, and signal quality over the wide bandwidth due to the use of a dual-loop PLL concept. The presented reconfigurable radar frontend module can be used with a single dual-polarized edge-launch square waveguide, or a centered TXRX waveguide plus two additional RX waveguide ports based on the same mmW PCB. The provided range and jitter measurements prove the high overall system measurement performance and stability. Additionally, a submillimeter XY-resolution and 2.7-mm depth Z-resolution SAR imaging system was presented.

ACKNOWLEDGMENT

This work was supported in part by the German Research Foundation (DFG) through Project TRR 196 MARIE under Grant 287022738 and in part by the Federal Ministry of Education and Research (BMBF) through Project PINK under Grant 16ME0176 K.

REFERENCES

- [1] C. Zeintl, F. Eibensteiner, and J. Langer, "Evaluation of FMCW radar for vibration sensing in industrial environments," in *Proc. IEEE 29th Int. Conf. Radioelektronika*, 2019, pp. 1–5.
- [2] S. Mohammadzadeh and F. Friederich, "Design of a quasioptical scanning system for a fast mobile FMCW terahertz imaging system," *J. Physics Conf. Ser.*, vol. 1537, no. 1, 2020, Art. no. 0 12017.
- [3] J. Schorlemer, C. Schulz, N. Pohl, I. Rolfes, and J. Barowski, "Compensation of sensor movements in short-range FMCW synthetic aperture radar algorithms," *IEEE Trans. Microw. Theory Techn.*, vol. 69, no. 11, pp. 5145–5159, Nov. 2021.
- [4] J. Barowski *et al.*, "Design and evaluation of a passive frequency-coded reflector using W-band FMCW radar," in *Proc. IEEE German Microw. Conf.*, 2020, pp. 92–95.
- [5] F. Michler, B. Scheiner, T. Reissland, R. Weigel, and A. Koelpin, "Micrometer sensing with microwaves: Precise radar systems for innovative measurement applications," *IEEE J. Microw.*, vol. 1, no. 1, pp. 202–217, Jan. 2021.
- [6] B. Hattenhorst, L. Piotrowsky, N. Pohl, and T. Musch, "An mmWave sensor for real-time monitoring of gases based on real refractive index," *IEEE Trans. Microw. Theory Techn.*, vol. 69, no. 11, pp. 5033–5044, Nov. 2021.
- [7] L. Piotrowsky, T. Jaeschke, S. Kueppers, J. Siska, and N. Pohl, "Enabling high accuracy distance measurements with FMCW radar sensors," *IEEE Trans. Microw. Theory Techn.*, vol. 67, no. 12, pp. 5360–5371, Dec. 2019.
- [8] J. Jebramcik, I. Rolfes, N. Pohl, and J. Barowski, "Millimeterwave radar systems for in-line thickness monitoring in pipe extrusion production lines," *IEEE Sens. Lett.*, vol. 4, no. 5, pp. 1–4, May 2020.
- [9] J. Barowski, T. Schultze, I. Willms, and I. Rolfes, "Monostatic and thickness-independent material characterisation based on microwave ellipsometry," in *Proc. IEEE German Microw. Conf.*, 2016, pp. 449–452.
- [10] J. Böck *et al.*, "SiGe HBT and BiCMOS process integration optimization within the DOTSEVEN project," in *Proc. IEEE Bipolar/BiCMOS Circuits Technol. Meeting*, 2015, pp. 121–124.
- [11] C. Bredendiek, K. Aufinger, and N. Pohl, "Full waveguide E- and W-band fundamental VCOs in SiGe:C technology for next generation FMCW radars sensors," in *Proc. 14th Eur. Microw. Integr. Circuits Conf.*, 2019, pp. 148–151.
- [12] N. Pohl, T. Jaeschke, and K. Aufinger, "An ultra-wideband 80 GHz FMCW radar system using a SiGe bipolar transceiver chip stabilized by a fractional-n PLL synthesizer," *IEEE Trans. Microw. Theory Techn.*, vol. 60, no. 3, pp. 757–765, Mar. 2012.
- [13] S. Kueppers, K. Aufinger, and N. Pohl, "A fully differential 100–140 GHz frequency quadrupler in a 130 nm SiGe:C technology for MIMO radar applications using the bootstrapped gilbert-cell doubler topology," in *Proc. IEEE 17th Topical Meeting Silicon Monolithic Integr. Circuits RF Syst.*, 2017, pp. 37–39.
- [14] Analog Devices, "ADF41513 integer-N/fractional-N PLL synthesizer," 2021. [Online]. Available: <https://www.analog.com/en/products/adf41513.html#product-documentation>
- [15] S. Hansen, C. Bredendiek, G. Briese, and N. Pohl, "D-band FMCW radar sensor for industrial wideband applications with fully-differential MMIC-to-RWG interface in SIW," in *Proc. IEEE MTT-S Int. Microw. Symp.*, Jun. 2022, pp. 1–4.
- [16] W. A. Ahmad *et al.*, "Multimode W-band and D-band MIMO scalable radar platform," *IEEE Trans. Microw. Theory Techn.*, vol. 69, no. 1, pp. 1036–1047, Jan. 2021.
- [17] A. Visweswaran *et al.*, "A 28-nm-CMOS based 145-GHz FMCW radar: System, circuits, and characterization," *IEEE J. Solid-State Circuits*, vol. 56, no. 7, pp. 1975–1993, Jul. 2021.
- [18] S. Kueppers, H. Cetinkaya, R. Herschel, and N. Pohl, "A compact 24 x 24 channel MIMO FMCW radar system using a substrate integrated waveguide-based reference distribution backplane," *IEEE Trans. Microw. Theory Techn.*, vol. 68, no. 6, pp. 2124–2133, Jun. 2020.
- [19] M. Kucharski, W. A. Ahmad, H. J. Ng, and D. Kissinger, "Monostatic and bistatic G-band BiCMOS radar transceivers with on-chip antennas and tunable TX-to-RX leakage cancellation," *IEEE J. Solid-State Circuits*, vol. 56, no. 3, pp. 899–913, Mar. 2021.
- [20] V. Issakov, A. Bilato, V. Kurz, D. Englisch, and A. Geiselbrechtinger, "A highly integrated D-band multi-channel transceiver chip for radar applications," in *Proc. IEEE BiCMOS Compound Semicond. Integr. Circuits Technol. Symp.*, 2019, pp. 1–4.
- [21] M. Hitzler *et al.*, "Ultracompact 160-GHz FMCW radar MMIC with fully integrated offset synthesizer," *IEEE Trans. Microw. Theory Techn.*, vol. 65, no. 5, pp. 1682–1691, May 2017.
- [22] M. Furqan, F. Ahmed, K. Aufinger, and A. Stelzer, "A D-band fully-differential quadrature FMCW radar transceiver with 11 dBm output power and a 3-dB 30-GHz bandwidth in SiGe BiCMOS," in *Proc. IEEE MTT-S Int. Microw. Symp.*, 2017, pp. 1404–1407.
- [23] A. Frischen, J. Hasch, D. Jetty, M. Girma, M. Gonser, and C. Waldschmidt, "A low-phase-noise 122-GHz FMCW radar sensor for distributed networks," in *Proc. Eur. Radar Conf.*, 2016, pp. 49–52.
- [24] T. Jaeschke, C. Bredendiek, S. Küppers, and N. Pohl, "High-precision D-band FMCW-radar sensor based on a wideband SiGe-transceiver MMIC," *IEEE Trans. Microw. Theory Techn.*, vol. 62, no. 12, pp. 3582–3597, Dec. 2014.
- [25] M. G. Girma, J. Hasch, M. Gonser, Y. Sun, and T. Zwick, "122 GHz single-chip dual-channel SMD radar sensor with integrated antennas for distance and angle measurements," in *Proc. 44th Eur. Microw. Conf.*, 2014, pp. 1754–1757.
- [26] H. Iqbal, C. Knill, M. Z. Khan, T. Chaloun, and C. Waldschmidt, "Polarimetric SAR for automotive applications," in *Proc. 15th Eur. Radar Conf.*, 2018, pp. 30–33.
- [27] N. Pohl, "A dielectric lens antenna with enhanced aperture efficiency for industrial radar applications," in *Proc. IEEE Middle East Conf. Antennas Propag.*, 2010, pp. 1–5.
- [28] *IEEE Standard for Rectangular Metallic Waveguides and Their Interfaces for Frequencies of 110 GHz and Above-Part 2: Waveguide Interfaces*, IEEE Standard 1785.2-2016, 2016.
- [29] A. Batra *et al.*, "Short-range SAR imaging from GHz to THz waves," *IEEE J. Microw.*, vol. 1, no. 2, pp. 574–585, Apr. 2021.
- [30] C. Liu, M. T. Al Qaseer, and R. Zoughi, "Permittivity extraction from synthetic aperture radar (SAR) images of multilayered media," *IEEE Trans. Instrum. Meas.*, vol. 70, pp. 1–11, 2021, doi: [10.1109/TIM.2021.3113118](https://doi.org/10.1109/TIM.2021.3113118).
- [31] J. Barowski, J. Jebramcik, J. Wagner, N. Pohl, and I. Rolfes, "Spatial identification of dielectric properties using synthetic aperture radar," in *Proc. IEEE MTT-S Int. Microw. Workshop Ser. Adv. Mater. Process. RF THz Appl.*, 2019, pp. 139–141.